

Quantum Amplitude-Amplification Eigensolver: A State-Learning-Assisted Approach beyond Energy-Gradient-Based Heuristics

Kyunghyun Baek,^{1,2} Seungjin Lee,³ Joonsuk Huh,^{4,2} Dongkeun Lee,⁵
Jinhyoung Lee,⁶ M. S. Kim,⁷ and Jeongho Bang^{1,2,*}

¹*Institute for Convergence Research and Education in Advanced Technology,
Yonsei University, Seoul 03722, Republic of Korea*

²*Department of Quantum Information, Yonsei University, Incheon 21983, Republic of Korea*

³*IMEC, Kapeldreef 75, Leuven, Belgium, 3001*

⁴*Department of Chemistry, Yonsei University, Seoul 03722, Republic of Korea*

⁵*Center for Quantum Information R&D, Korea Institute of Science
and Technology Information, Daejeon 34141, Republic of Korea*

⁶*Department of Physics, Hanyang University, Seoul, 04763, Republic of Korea*

⁷*Blackett Laboratory, Imperial College London, London SW7 2AZ, United Kingdom*

(Dated: November 18, 2025)

Ground-state estimation lies at the heart of a broad range of quantum simulations. Most near-term approaches are cast as variational energy minimization and thus inherit the challenges of problem-specific energy landscapes. We develop the quantum amplitude-amplification eigensolver (QAAE), which departs from the variational paradigm and instead coherently drives a trial state toward the ground state via quantum amplitude amplification. Each amplitude-amplification round interleaves a reflection about the learned trial state with a controlled short-time evolution under a normalized Hamiltonian; an ancilla readout yields an amplitude-amplified pure target state that a state-learning step then re-encodes into an ansatz circuit for the next round—without evaluating the energy gradients. Under standard assumptions (normalized \hat{H} , a nondegenerate ground-state, and a learning update), the ground-state overlap increases monotonically per round and the procedure converges; here, a per-round depth bound in terms of the ansatz depth and Hamiltonian-simulation cost establishes hardware compatibility. Cloud experiments on IBMQ processor verify our amplification mechanism on a two-level Hamiltonian and a two-qubit Ising model, and numerical benchmarks on H_2 , LiH , and a 10-qubit longitudinal-and-transverse-field Ising model show that QAAE integrates with chemistry-inspired and hardware-efficient circuits and can surpass gradient-based VQE in accuracy and stability. These results position QAAE as a variational-free and hardware-compatible route to ground-state estimation for near-term quantum simulation.

I. INTRODUCTION

Estimating the ground state of an interacting many-body Hamiltonian is central to quantum simulation [1]. However, accurate ground-state determination is formidable: the Hilbert space grows exponentially with the number of orbitals (or qubits), and the local Hamiltonian problem is QMA-hard [2]. Classical modern numerics beyond exact diagonalization exploit structures but face intrinsic limits. For example, Tensor-network techniques (e.g., DMRG/MPS, TEBD) perform well for area-law states, but the required bond dimension swells with entanglement and/or long-range couplings, rapidly increasing the cost [3–5]. Stochastic schemes (e.g., quantum Monte-Carlo) are efficient only in sign-problem-free cases [6]. Thus, for strongly correlated and/or higher-dimensional systems, these tools often lose accuracy or require prohibitive resources.

Meanwhile, quantum algorithms promise advantages. Chief among them is quantum phase estimation (QPE), which—given a trial state with nonzero ground-state overlap—projects onto an eigenstate and estimates its

energy with Heisenberg-limited precision [7–10]. However, QPE-based eigensolvers require an m -qubit phase register for $\mathcal{O}(2^{-m})$ resolution, long sequences of multi-controlled-unitary evolutions, and an inverse quantum Fourier transform (or semi-classical variants) in practice. For generic many-body Hamiltonians, this QPE circuit incurs accuracy-dependent overhead [11, 12]; the resulting depth and fidelity typically exceed the near-term capabilities. Iterative or Bayesian QPE can reduce ancillas, but still demands long circuit depths, and the success probability hinges on the initial overlap—often prompting amplitude amplification or tailored preparation, further increasing the implementation depth [13–15]. Thus, QPE remains the asymptotic gold standard, but its practical realization is expected to await the fault-tolerant architectures with robust quantum error correction, motivating hardware-conscious alternatives in the interim.

Very recently, more resource-efficient and near-term realizable approaches have emerged as candidates for tangible quantum advantage [16, 17]. Foremost among them is the variational quantum eigensolver (VQE) [18–20], which leverages the variational principle $\langle \Psi | \hat{H} | \Psi \rangle \geq \lambda_0$ to recast ground-state estimation [21, 22]:

$$\min_{\theta} E(\theta) := \langle \Psi(\theta) | \hat{H} | \Psi(\theta) \rangle, \quad (1)$$

* jbang@yonsei.ac.kr

where λ_0 is the ground-state energy of a given Hamiltonian \hat{H} and the trial state $|\Psi(\boldsymbol{\theta})\rangle$ is prepared by a parametric quantum circuit, often-called ansatz; the parameter vector $\boldsymbol{\theta}$ is updated by a classical optimizer. In practice, \hat{H} is decomposed as $\hat{H} = \sum_{l=1}^L w_l \hat{P}_l$ (e.g., Pauli strings or few-body terms), the expectation $E(\boldsymbol{\theta})$ is estimated from repeated measurements, and gradients are obtained via parameter-shift or finite-difference rules, yielding a classical-quantum hybrid interplay [23].

Despite many proof-of-concept successes, the VQE framework faces obstacles. (i) Local minima: Finite-shot noise and hardware imperfections yield nonconvex objectives, making convergence sensitive to initialization [24, 25]. (ii) Barren plateaus: For sufficiently expressive or randomly initialized ansatz, the energy-gradient variance can vanish exponentially with system size [26–29]. The noises can further induce plateauing [30]. (iii) Expressivity-vs-trainability trade-off: Chemistry-inspired ansatz (e.g., UCCSD/ADAPT-type) mitigates plateaus but incurs large parameter counts; hardware-efficient circuits are shallow, yet often harder to train [31, 32]. (iv) Measurement overhead: Shot complexity scales with estimator variance and the number of Hamiltonian terms [33, 34]. Collectively, these factors limit the reliability of the variational methods and motivate alternative algorithms that avoid explicit energy-landscape search based on energy-gradient, while offering convergence guarantees under hardware-aware resource bounds.

In this work, we develop the quantum amplitude-amplification eigensolver (QAAE), that coherently steers a trial state toward the ground state. Each round applies a reflection about the learned trial state and a short-time controlled evolution under a normalized Hamiltonian; an ancilla readout yields an amplitude-amplified pure state that is re-encoded into an ansatz circuit for the next round—*without* evaluating the energy gradients. This amplify–learn loop increases the ground-state overlap while avoiding the exploration of rugged Hamiltonian landscapes and can mitigate gradient-pathologies typical of variational heuristics. We validate this amplification mechanism on IBMQ processor (a two-level Hamiltonian and a two-qubit Ising model), and benchmark QAAE on H_2 (4 qubits), LiH (12 qubits), and longitudinal-and-transverse-field Ising model (10 qubits), where the chemistry-inspired and hardware-efficient PQCs integrate naturally. In particular, the benchmark on 10-qubit Ising model attains higher accuracy and reliability than VQE under matched resources.

II. QUANTUM AMPLITUDE AMPLIFICATION EIGENSOLVER

To implement QAAE, we start by preparing a trial state, denoted as $|\Psi(\boldsymbol{\theta})\rangle$. Here, $\boldsymbol{\theta}$ is a vector consisting of the adjustable parameters θ_j ($j = 0, 1, \dots, K-1$): i.e., $\boldsymbol{\theta} = (\theta_0, \theta_1, \dots, \theta_{K-1})^T$. The trial-state encoding is

performed by using an ansatz, denoted as $\hat{A}(\boldsymbol{\theta})$, such that

$$|\Psi(\boldsymbol{\theta})\rangle = |+\rangle \otimes |\alpha(\boldsymbol{\theta})\rangle = |+\rangle \otimes \hat{A}(\boldsymbol{\theta})|0\rangle, \quad (2)$$

where $|0\rangle = |0\rangle^{\otimes q}$ and q is the number of qubits to model the given (2^q -dimensional) Hamiltonian \hat{H} . Here, the ansatz-estimated ground state $|\alpha(\boldsymbol{\theta})\rangle = \hat{A}(\boldsymbol{\theta})|0\rangle$ is expected to evolve towards the true ground state. The single-qubit ancilla state $|+\rangle = \frac{1}{\sqrt{2}}(|0\rangle + |1\rangle)$ is used for the stability of the process [35]. Then, we introduce a unitary process associated with a normalized Hamiltonian \hat{H} (i.e., the eigenvalues are in $(0, 1]$), defined as

$$\hat{U} = \sum_{k=0,1} i^k |k\rangle\langle k| \otimes e^{(-1)^k i\omega\hat{H}}, \quad (3)$$

which is supposed to be designed efficiently [12, 36]. Here, ω is set to be $\frac{\pi}{4}$. With this unitary \hat{U} , we can define an operation for a single round of the amplification as

$$\hat{T}(\boldsymbol{\theta}) = \hat{R}(\boldsymbol{\theta})\hat{U}\hat{R}(\boldsymbol{\theta})\hat{U}^\dagger, \quad (4)$$

where $\hat{R}(\boldsymbol{\theta}) = \hat{\mathbb{1}} - 2|\Psi(\boldsymbol{\theta})\rangle\langle\Psi(\boldsymbol{\theta})|$, often-called Householder reflection [37–39]. Given a set of the parameters $\boldsymbol{\theta}$, $\hat{R}(\boldsymbol{\theta})$ can be implemented by using $\hat{A}(\boldsymbol{\theta})$ and $\hat{A}^\dagger(\boldsymbol{\theta})$. Schematic of the setup is depicted in Fig. 1.

Amplify–Learn loop.—We describe how QAAE process runs. The process comprises the two essential steps:

(A.1) Amplify: $\hat{T}(\boldsymbol{\theta})$ is applied to $|\Psi(\boldsymbol{\theta})\rangle$ for chosen $\boldsymbol{\theta}$. Subsequently, by performing the projection measurement $\hat{P}_k = |k\rangle\langle k|$ ($k \in \{0, 1\}$) on the ancillary qubit, we have the output state as

$$|\varphi_{\text{out},k}\rangle = \frac{\langle k|\hat{T}(\boldsymbol{\theta})|\Psi(\boldsymbol{\theta})\rangle}{\sqrt{p_k}}, \quad (5)$$

where p_k is the probability of measuring $|k\rangle$, with the calculated value of $\frac{1}{2}$. The state $|\varphi_{\text{out},k}\rangle$ becomes closer to the ground state compared to $|\alpha(\boldsymbol{\theta})\rangle$ (as shown later).

(A.2) Learn: The trial state and $\hat{T}(\boldsymbol{\theta})$ are reconfigured by the parameter updates: $\boldsymbol{\theta} \rightarrow \boldsymbol{\theta}'$. The main idea is to use $|\varphi_{\text{out},k}\rangle$ in the new trial state, enabling the step **(A.1)** to reproduce an output closer to the ground state. To realize this idea, we prepare a next-round trial state

$$|\alpha(\boldsymbol{\theta}')\rangle = \hat{A}(\boldsymbol{\theta}')|0\rangle = |\varphi_{\text{out},k}\rangle \quad (6)$$

with the updated $\boldsymbol{\theta}'$; thus, we have to learn $|\varphi_{\text{out},k}\rangle$. We formulate the task of learning $|\varphi_{\text{out},k}\rangle$ as:

$$\text{opt}_{\boldsymbol{\theta}} \mathcal{F}(\boldsymbol{\theta}), \text{ subject to } \boldsymbol{\theta} \in \Theta, \quad (7)$$

where $\text{opt}_{\boldsymbol{\theta}} \in \{\arg \max_{\boldsymbol{\theta}}, \arg \min_{\boldsymbol{\theta}}\}$, $\mathcal{F}(\boldsymbol{\theta})$ is an objective function, and Θ represents a parameter space. The size and landscape of Θ depends on the underlying structure of the learning $\hat{A}(\boldsymbol{\theta})$ [40]. Crucially, the learning target is a fixed pure state rather than an energy functional; hence, no energy-gradient-based heuristics are employed.

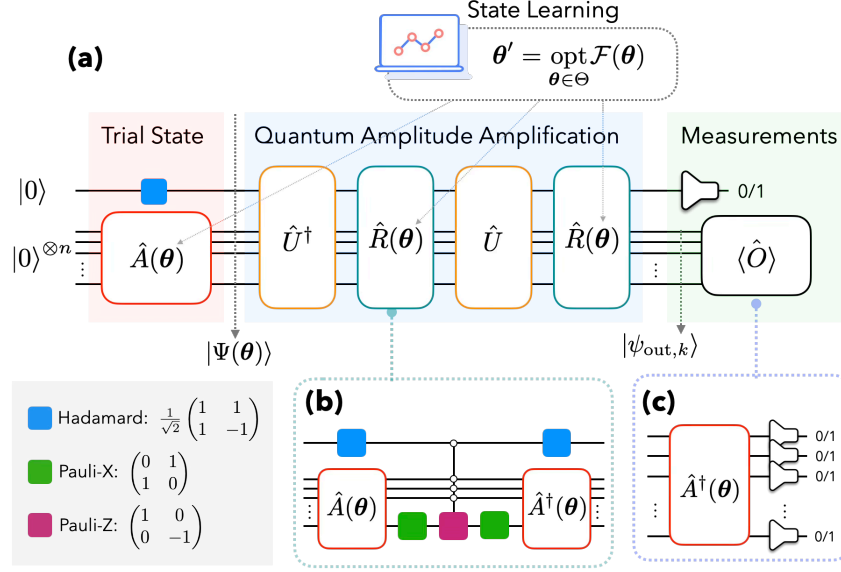


FIG. 1. Schematic of our QAAE setup. (a) The circuits for generating the trial state $|\Psi(\theta)\rangle$ and implementing the ground-state amplitude amplification $\hat{T}(\theta)$. (b) The reflecting operation $\hat{R}(\theta)$ is implemented by using $\hat{A}(\theta)$ and some fundamental gates (Hadamard, Pauli-X ($\hat{\sigma}_x$), Pauli-Z ($\hat{\sigma}_z$), and q -Toffoli, etc.). (c) The state-learning [as in Eq. (7)] is performed for $|\varphi_{\text{out},k}\rangle$. Then, a new vector θ' is identified and the circuit elements $\hat{A}(\theta)$ and $\hat{R}(\theta)$ are (re)dialled: $\theta \rightarrow \theta'$.

An iteration of (A.1)–(A.2) yields a sequence whose ground-state overlap increases round by round. A practical halting rule compares the successive-round energies or output-state overlaps. If the process does not halted within a maximum round/shot budget, it returns “task failure.” The detailed line-by-line algorithmic description of our QAAE process is presented in **Algorithm 1**.

Algorithm 1 Our QAAE process

Require: $|0\rangle, |+\rangle, \hat{A}(\theta), \hat{A}^\dagger(\theta), \hat{U}, \hat{U}^\dagger, \hat{R}_0, \hat{P}_k$

- 1: Task: Given Hamiltonian \hat{H} , find its ground state $|\lambda_0\rangle$
- 2: Initialize:
- 3: $|0\rangle = |0\rangle^{\otimes q}, \hat{R}_0 = \hat{\mathbb{1}} - 2|0\rangle\langle 0|$
- 4: $iter = 0, halt \leftarrow \emptyset, \Xi \leftarrow$ an arbitrary large number
- 5: $\theta \leftarrow \{Rand(\theta_j)\}$ ▷ $Rand(\cdot)$: Random function
- 6: **while** $halt = \emptyset$ AND $iter < \Xi$ **do**
- 7: $|\Psi(\theta)\rangle \leftarrow |+\rangle \otimes \hat{A}(\theta)|0\rangle$
- 8: $\hat{T}(\theta) \leftarrow \hat{R}(\theta)\hat{U}\hat{R}(\theta)\hat{U}^\dagger$ where $\hat{R}(\theta) = \hat{A}(\theta)\hat{R}_0\hat{A}^\dagger(\theta)$
- 9: Apply $\hat{T}(\theta)$ to $|\Psi(\theta)\rangle$
- 10: Measurement $\hat{P}_k = |k\rangle\langle k|$ ($k = 0, 1$)
- 11: Obtain the output state $|\varphi_{\text{out},k}\rangle$ ▷ see Eq. (5)
- 12: **if** $k = 0$ (or $k = 1$) **then**
- 13: State learning: $\theta' = \text{opt}_{\theta \in \Theta} \mathcal{F}(\theta)$
- 14: **end if**
- 15: **if** halting condition is met **then**
- 16: $halt \leftarrow True$
- 17: **end if**
- 18: $\theta \leftarrow \theta'$
- 19: $iter \leftarrow iter + 1$
- 20: **end while**
- 21: **if** $iter \geq \Xi$ **then return** “algorithm failure”
- 22: **end if**
- 23: **return** θ and $|\varphi_{\text{out},k}\rangle$ ($\simeq |\lambda_0\rangle$) ▷ Solution

III. THEORETICAL ANALYSIS

A. Converging behavior

We analyze the amplify–learn loop by reminding the (A.1) amplify and (A.2) learn steps. Throughout, we assume a normalized Hamiltonian \hat{H} with a nondegenerate ground state $0 < \lambda_0 < \lambda_1 \leq \dots \leq \lambda_{2^q-1} \leq 1$, the ancilla prepared in $|+\rangle$, and the controlled short-time evolution \hat{U} as in Eq. (3) with the evolution-time parameter $\omega = \frac{\pi}{4}$; reflections and one-round operator are as in Eqs. (2)–(4).

Amplify: one-step improvement.—Let the system trial state be decomposed in the eigenbasis as

$$|\alpha(\theta)\rangle = \sum_{j=0}^{d-1} \gamma_j |\lambda_j\rangle, \quad \Gamma_{|\psi\rangle} := |\langle \lambda_0 | \psi \rangle|^2, \quad (8)$$

where $d = 2^q$. Define the transition amplitude:

$$\mathcal{W} := \langle +, \alpha(\theta) | \hat{U} | +, \alpha(\theta) \rangle = |\mathcal{W}| e^{i\frac{\pi}{4}}. \quad (9)$$

Here, $|\mathcal{W}| = \sum_{j=0}^{d-1} |\gamma_j|^2 \cos \tilde{\lambda}_j$ with $\tilde{\lambda}_j := \frac{\pi}{4}(1 - \lambda_j)$. The normalized post-measurement system state for outcome $k \in \{0, 1\}$ is [Eq. (5)]

$$|\varphi_{\text{out},k}\rangle = \frac{\langle k | \hat{T}(\theta) | \Psi(\theta) \rangle}{\sqrt{p_k}}, \quad p_k = \frac{1}{2}. \quad (10)$$

Then, we present the following proposition and provide its proof:

Proposition 1 (Ground-state amplitude amplification). Assume $0 < \Gamma_{|\alpha(\theta)\rangle} < 1$. For each $k \in \{0, 1\}$, the step **(A.1)** strictly increases the ground-state amplitude:

$$\begin{aligned} \delta_{\lambda_0} &:= \Gamma_{|\varphi_{\text{out},k}\rangle} - \Gamma_{|\alpha(\theta)\rangle} = 4|\mathcal{W}|\chi\xi_0|\gamma_0|^2 \\ &\geq c_\star \Gamma_{|\alpha(\theta)\rangle} (1 - \Gamma_{|\alpha(\theta)\rangle}) > 0, \end{aligned} \quad (11)$$

where

$$\begin{aligned} \chi &:= 4|\mathcal{W}|^2 - 1, \\ \xi_j &:= |\mathcal{W}| - \cos \tilde{\lambda}_j, \\ c_\star &:= 4 \cos \tilde{\lambda}_0 (4 \cos^2 \tilde{\lambda}_0 - 1) (\cos \tilde{\lambda}_1 - \cos \tilde{\lambda}_0) > 0. \end{aligned} \quad (12)$$

Proof. — A direct calculation (expanding in the eigenbasis and using Eq. (3) and Eq. (4)) gives the coefficient update

$$\gamma_j \Rightarrow \gamma'_j = \begin{cases} (4|\mathcal{W}|^2 - 2\mathcal{W}^* e^{i\omega\lambda_j} - 1)\gamma_j, & k = 0, \\ (4|\mathcal{W}|^2 - 2i\mathcal{W}^* e^{-i\omega\lambda_j} - 1)\gamma_j, & k = 1, \end{cases} \quad (13)$$

where $|\gamma'_j|^2 = (1 + 4|\mathcal{W}|\chi\xi_j)|\gamma_j|^2$. Thus, we get $\delta_{\lambda_0} = 4|\mathcal{W}|\chi\xi_0|\gamma_0|^2$. Here, the normalization follows from

$$\sum_j \xi_j |\gamma_j|^2 = |\mathcal{W}| - \sum_j |\gamma_j|^2 \cos \tilde{\lambda}_j = 0. \quad (14)$$

Since $\lambda_0 < \lambda_1 \leq \dots \leq \lambda_{d-1}$, we have

$$\cos \tilde{\lambda}_0 \leq |\mathcal{W}| \leq \cos \tilde{\lambda}_{d-1}, \quad (15)$$

and hence,

$$\begin{aligned} \chi &\geq 4 \cos^2 \tilde{\lambda}_0 - 1 \geq 1, \\ \xi_0 &= \sum_{j \geq 1} |\gamma_j|^2 (\cos \tilde{\lambda}_j - \cos \tilde{\lambda}_0) > 0. \end{aligned} \quad (16)$$

Substituting the respective lower bounds for $|\mathcal{W}|$ and χ establishes Eq. (11); the inequality is valid for all non-trivial cases with $0 < \Gamma_{|\alpha(\theta)\rangle} < 1$. \square

We clarify that the result does not assume any particular expressivity of $\hat{A}(\theta)$ beyond defining the current trial state; in fact, expressivity matters in **(A.2)**.

Learn: state learning and stability.— Given $|\varphi_{\text{out},k}\rangle$ from **(A.1)**, the next trial is obtained by solving the state-learning problem:

$$\theta' = \text{opt}_{\theta \in \Theta} \mathcal{F}(\theta), \quad |\alpha(\theta')\rangle = \hat{A}(\theta')|0\rangle \simeq |\varphi_{\text{out},k}\rangle, \quad (17)$$

with \mathcal{F} an overlap/distance-based objective estimated from suitable observables; for example, maximize $|\langle \alpha(\theta) | \varphi_{\text{out},k} \rangle|^2$ or minimize the trace distance $D(\hat{\rho}_\theta, \hat{\rho}_{\text{out},k})$ where

$$D = \frac{1}{2} \|\hat{\rho}_\theta - \hat{\rho}_{\text{out},k}\|_1. \quad (18)$$

Because the target is a *fixed pure state* rather than an energy functional, **(A.2)** avoids explicit exploration

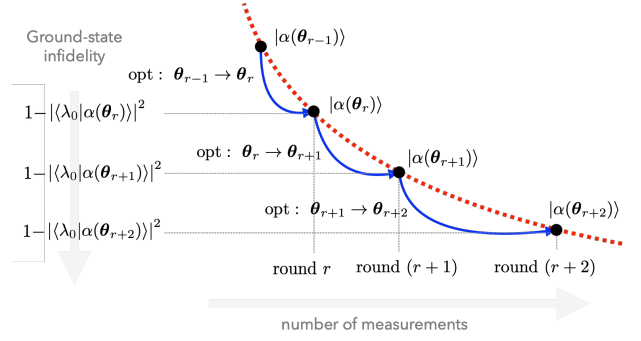


FIG. 2. The predicted behavior of converging to the ground state in our QAAE. Let us start by a system output state $|\varphi_{\text{out},k}(r)\rangle$ at any r -th round, which is closer to the ground state than those from the previous rounds. At this round, the state learning is completed and the control parameter vector is updated as $\theta_r \rightarrow \theta_{r+1}$, and the PQC states $|\alpha(\theta_{r+1})\rangle$ is prepared (see the blue solid line). By iterating these processes, the PQC states evolves into the ground state, which is depicted as a trajectory along the red dashed line.

of rugged energy landscapes and admits well-studied smooth barrier or trust-region designs, e.g., using

$$\mathcal{F} = D^2 - \log(1 - D^2) \text{ on } D \in [0, 1) \quad (19)$$

for conditioning [41].

The key property needed for convergence is stability of the ground-state weight under learning error. Thus, we provide the following lemma:

Lemma 1 (Stability under learning error). Let $\hat{\rho}_{\text{out},k} = |\varphi_{\text{out},k}\rangle \langle \varphi_{\text{out},k}|$ and $\hat{\rho}_{\theta'} = |\alpha(\theta')\rangle \langle \alpha(\theta')|$. Then, for the projector $\hat{\Pi}_0 = |\lambda_0\rangle \langle \lambda_0|$,

$$|\delta_{\lambda_0}| = \left| \text{Tr}[\hat{\Pi}_0(\hat{\rho}_{\text{out},k} - \hat{\rho}_{\theta'})] \right| \leq D(\hat{\rho}_{\text{out},k}, \hat{\rho}_{\theta'}). \quad (20)$$

Proof. — For any POVM element $0 \leq \hat{\Pi} \leq \hat{\mathbb{1}}$, the following holds:

$$\left| \text{Tr}[\hat{\Pi}(\hat{\rho} - \hat{\rho}')] \right| \leq \frac{1}{2} \|\hat{\rho} - \hat{\rho}'\|_1 = D(\hat{\rho}, \hat{\rho}'). \quad (21)$$

Taking $\hat{\Pi} = \hat{\Pi}_0$ gives Eq. (20). \square

Combining **Proposition 1** with **Lemma 1** yields a per-round bound. Let $g_r := \Gamma_{|\alpha(\theta_r)\rangle}$ and $\varepsilon_r := D(|\alpha(\theta_{r+1})\rangle, |\varphi_{\text{out},k}(r)\rangle)$ denote the learning error at round r . Then,

$$g_{r+1} \geq g_r + c_\star g_r (1 - g_r) - \varepsilon_r. \quad (22)$$

In particular: (i) Exact learning (i.e., $\varepsilon_r = 0$) gives a strictly increasing, bounded sequence with logistic-type gain, hence g_r approaches 1. (ii) Approximate learning preserves monotonicity whenever $\varepsilon_r < c_\star g_r (1 - g_r)$; if $\varepsilon_r \rightarrow 0$ (or $\sum_r \varepsilon_r < \infty$), the sequence still converges to 1. Figure 2 illustrates the predicted trajectory.

Convergence via amplify-learn.—The amplify step provides a state-independent improvement mechanism (**Proposition 1**) whose strength is set by spectral constants of \hat{H} via $c_\star > 0$, while the learn step translates this improvement into the next round within the chosen ansatz class, with the robustness quantified by Eq. (20). Note that our QAAE operates outside the variational paradigm: it neither navigates rugged Hamiltonian energy landscapes nor depends on energy gradients. Robustness to imperfect learning is quantified by the stability bound in Eq. (20), which, combined with the per-round overlap gain, yields the recursion Eq. (22) (with $g_r = \Gamma_{|\alpha(\theta_r)}$) and $\varepsilon_r = D(\hat{\rho}_{\theta_{r+1}}, \hat{\rho}_{\text{out},k})$. Under the standard assumptions and faithful (or asymptotically faithful) learning, this establishes a *provably monotone and convergent* route to the ground state.

B. Circuit Depth

We bound the circuit depth per QAAE round. Each round comprises: (i) trial-state preparation $\hat{A}(\theta)$, (ii) the Householder reflection $\hat{R}(\theta)$ about $|\Psi(\theta)\rangle$, and (iii) the controlled short-time evolution \hat{U} . Denote their depths by \mathcal{D}_A , \mathcal{D}_R , and \mathcal{D}_U , respectively.

Proposition 2 (Per-round circuit depth). *For a normalized Hamiltonian \hat{H} and \hat{U} in Eq. (3) with fixed ω , one QAAE round has circuit depth*

$$\mathcal{D}_{\text{round}} \leq \mathcal{D}_A + 2(\mathcal{D}_R + \mathcal{D}_U), \quad (23)$$

with

$$\mathcal{D}_R \leq 2\mathcal{D}_A + \mathcal{O}(q), \quad \mathcal{D}_U = \mathcal{O}(\text{poly}(q)\varepsilon_H^{-\frac{1}{2\kappa}}), \quad (24)$$

where q is the number of system qubits, ε_H is the target simulation accuracy for $e^{-i\omega\hat{H}}$, and 2κ is the order of a Trotter-Suzuki product formula (other short-time simulation primitives may be used). Consequently,

$$\mathcal{D}_{\text{round}} \leq 5\mathcal{D}_A + 2\mathcal{D}_U + \mathcal{O}(q). \quad (25)$$

Proof sketch.—Using the canonical construction $\hat{R}(\theta) = (\text{Hadamard} \otimes \hat{A}(\theta))\hat{R}_0(\text{Hadamard} \otimes \hat{A}(\theta))^\dagger$ with $\hat{R}_0 = \hat{\mathbb{1}} - 2|\mathbb{0}\rangle\langle\mathbb{0}|$ (as illustrated in Fig. 1(b)), the reflection depth is that of $\hat{A}(\theta)$, its adjoint $\hat{A}(\theta)^\dagger$, an ancilla Hadamard, and a $(q+1)$ -controlled phase (a relative-phase multi-controlled Z). Here, standard decompositions give depth $\mathcal{O}(q)$ for this multi-controlled gate; with an extra ancilla, $\mathcal{O}(\log q)$ is possible while keeping width $\mathcal{O}(q)$ [42]. Hence, $\mathcal{D}_R \leq 2\mathcal{D}_A + \mathcal{O}(q)$.

For $e^{-i\omega\hat{H}}$ with fixed $\omega = \frac{\pi}{4}$, a 2κ -th order product formula over $\hat{H} = \sum_{l=1}^L \hat{h}_l$ yields the step cost $\mathcal{O}(L)$ and step count $\nu = \mathcal{O}((L\omega)^{1+1/2\kappa}\varepsilon_H^{-1/2\kappa})$ [43]. For typical local models $L = \text{poly}(q)$, so $\mathcal{D}_U = \mathcal{O}(\text{poly}(q)\varepsilon_H^{-1/2\kappa})$. The controlization adds only constant-factor overhead for

Pauli-string terms and can be scheduled with pre/post controlled Paulis [44].

One round of QAAE executes state preparation once and the pattern $\hat{R}\hat{U}\hat{R}\hat{U}^\dagger$, giving Eq. (23). Substituting Eq. (24) yields Eq. (25). \square

Hardware-conscious design.—Now we remark the following. (i) Ansatz modularity: The bound in Eq. (25) separates the ansatz cost \mathcal{D}_A from Hamiltonian simulation \mathcal{D}_U . Chemistry-inspired circuits (e.g., UCC-type) and hardware-efficient layouts both fit this template; thus QAAE inherits their depth-scaling properties [45]. (ii) Parallel scheduling: For local Hamiltonians, the Pauli terms partition into commuting layers; with standard graph colorings of the interaction hyper-graph, one obtains constant (model-dependent) parallel depth per Trotter step, improving the constant in $\text{poly}(q)$ without changing the asymptotics. Controlled-Pauli “wraps” can be hoisted and canceled across layers to reduce two-qubit gate count [44]. (iii) Beyond Trotter: LCU/QSP-based short-time simulation achieves asymptotically better accuracy dependence but typically requires block-encoding and additional ancillas; for NISQ/early-FTQC contexts, product formulas often yield lower overheads [46–50]. Either choice plugs into Eq. (23) by substituting the corresponding \mathcal{D}_U . (iv) Controlled- Z fan-in: The $\mathcal{O}(q)$ term in Eq. (24) stems from the $(q+1)$ -controlled phase in \hat{R}_0 ; the depth can be reduced to $\mathcal{O}(\log q)$ with an ancilla ladder at the cost of a small qubit overhead [42]. (v) Error budgeting: Because QAAE’s per-round gain is set by spectral constants (**Proposition 1**), the simulation accuracy ε_H needs only be tight enough that Trotter error remains below this gain; thus \mathcal{D}_U can be chosen by a simple budget rule rather than by the stringent precision targets common in phase-estimation pipelines.

Overall, Eqs. (23)–(25) show that the amplify-learn loop admits a *polynomial* per-round circuit depth governed by the chosen ansatz and short-time simulation primitive, underscoring QAAE’s hardware compatibility.

IV. APPLICATIONS

A. Motivating example: a two-level system Hamiltonian

To isolate and validate the core mechanism of QAAE, we consider the physically universal qubit Hamiltonian

$$\hat{H}_{2L} = \alpha\hat{\mathbb{1}} + \mathbf{r} \cdot \hat{\boldsymbol{\sigma}} \quad \text{with} \quad \hat{\boldsymbol{\sigma}} = (\hat{\sigma}_x, \hat{\sigma}_y, \hat{\sigma}_z)^T, \quad (26)$$

whose spectrum is $\lambda_{0,1} = \alpha \mp |\mathbf{r}|$ with the energy gap $d = \lambda_1 - \lambda_0 = 2|\mathbf{r}|$. Equivalently,

$$\hat{H}_{2L} = \lambda_0\hat{\mathbb{1}} + d|\lambda_1\rangle\langle\lambda_1|, \quad (27)$$

where $\{|\lambda_0\rangle, |\lambda_1\rangle\}$ are unknown. This archetypal two-level model cleanly probes whether a single QAAE round coherently amplifies the ground-state weight as

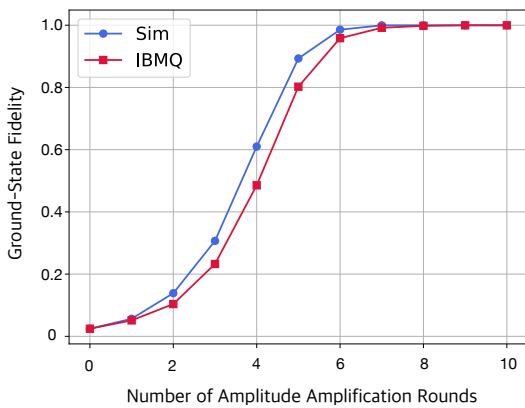


FIG. 3. Ground-state fidelity vs. number of QAAE rounds for the two-level Hamiltonian. Both Qiskit emulation and `ibm_yonsei` experiments show monotone improvement consistent with **Proposition 1**.

predicted by **Proposition 1**, without confounding effects from complex many-body structure. Crucially, we deliberately disable the state-learning here: the next trial is obtained by characterizing the post-measurement output via a small set of observables, so that any improvement can be attributed purely to the amplitude amplification.

For a general q -qubit ansatz, we expand

$$\hat{\rho}(\theta) = |\alpha(\theta)\rangle \langle \alpha(\theta)| = \frac{1}{2^q} \sum_{\mathbf{v} \in \mathcal{I}} C_{\mathbf{v}}(\theta) \bigotimes_{j=1}^q \hat{\sigma}_{v_j}, \quad (28)$$

where $v_j \in \{0, 1, 2, 3\}$, with $\hat{\sigma}_0 = \hat{\mathbb{1}}$, $\hat{\sigma}_1 = \hat{\sigma}_x$, $\hat{\sigma}_2 = \hat{\sigma}_y$, and $\hat{\sigma}_3 = \hat{\sigma}_z$. The index string $\mathbf{v} = v_1 v_2 \dots v_q$ specifies a q -qubit Pauli string, and the index set $\mathcal{I} \subseteq \{0, 1, 2, 3\}^q$ defines the subset of Pauli strings contributing to the expansion: i.e., $\{\bigotimes_j \hat{\sigma}_{v_j}\}_{\mathbf{v} \in \mathcal{I}}$, where $|\mathcal{I}| \ll 4^q$ in practice. The coefficients $C_{\mathbf{v}}(\theta)$ depend on the parameters θ and encode the structure of the ansatz-generated state in the Pauli basis. In the present single-qubit case ($q=1$), we restrict to the x - z meridian and use

$$\hat{\rho}(\theta) = \frac{1}{2} (\hat{\mathbb{1}} + C_x(\theta) \hat{\sigma}_x + C_z(\theta) \hat{\sigma}_z), \quad (29)$$

with $C_x(\theta) = \sin \theta$ and $C_z(\theta) = \cos \theta$. Each round measures $\{\hat{\sigma}_x, \hat{\sigma}_z\}$ on the output state $|\varphi_{\text{out},k}\rangle$ of **(A.1)**, forming $\mathbf{c} = (c_x = \langle \hat{\sigma}_x \rangle, c_z = \langle \hat{\sigma}_z \rangle)$. We then project to the Bloch sphere by normalization $\tilde{\mathbf{c}} = \mathbf{c}/|\mathbf{c}|$ (a maximum-likelihood pure-state update under isotropic noise) and set the next trial by $\theta' = \text{atan2}(\tilde{c}_x, \tilde{c}_z)$, thereby re-encoding the amplified state without evaluating the variational gradients.

We then implement the single-ancilla QAAE round on the IBMQ cloud processor “`ibm_yonsei`” and compare to a Qiskit-based local emulator. The initial trial has very low ground-state fidelity (lower than 0.024 on average). Figure 3 shows that the fidelity increases steadily toward unity as the number of amplification rounds grows, confirming **Proposition 1** on hardware. In Fig. 4, orange

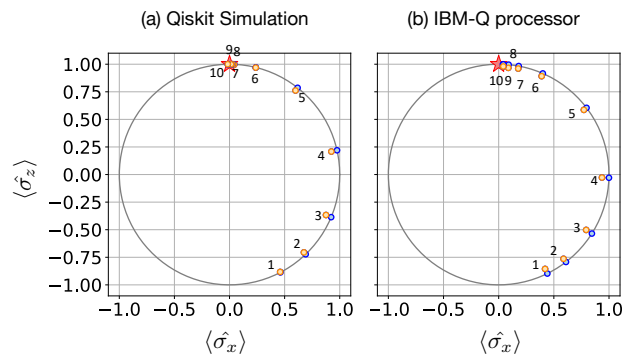


FIG. 4. Expectation values $\langle \hat{\sigma}_x \rangle$ and $\langle \hat{\sigma}_z \rangle$ from (a) Qiskit emulation and (b) `ibm_yonsei` experiments (orange), and corresponding normalized Bloch vectors used for re-encoding (blue). The red star marks the ground state. The normalization projects noisy Bloch vectors back to purity, mitigating isotropic-type noise and improving update robustness.

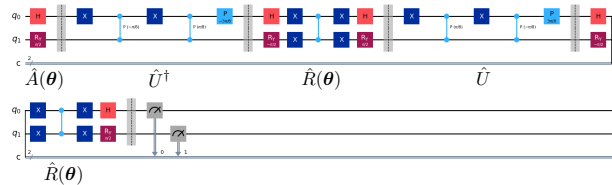


FIG. 5. Single-ancilla QAAE circuit for the two-level Hamiltonian. One round consists of the reflection–evolution–reflection–inverse-evolution pattern of Sec. II, followed by ancilla measurement and re-encoding of the amplified pure state.

dots are raw expectation values ($\langle \hat{\sigma}_x \rangle, \langle \hat{\sigma}_z \rangle$) from (a) emulation and (b) experiment; blue dots are the normalized Bloch vectors used for re-encoding. Their close alignment indicates that the simple normalization step acts as an effective denoiser against approximately isotropic noise, stabilizing the round-to-round parameter update. The ground state (red star) is approached monotonically under repeated amplification. Circuit-level details for this one-qubit instance are shown in Fig. 5.

Although \hat{H}_{2L} acts on a single qubit, it is the canonical normal form of any effective two-level subspace (e.g., avoided crossings, spin-1/2 in a field). Here, the energy gap d sets the constant governing the per-round improvement in **Proposition 1**, and the experiment demonstrates that QAAE’s amplitude amplification translates into observable, monotone fidelity gains on real hardware—without invoking the variational principle or exploring an energy landscape. The same observable-driven re-encoding idea scales: for larger q , one may replace $\{\hat{\sigma}_x, \hat{\sigma}_z\}$ by a Pauli set as in Eq. (28) and exploit entangled measurements [51] or classical-shadow estimation [52] to keep the circuit cost practical.

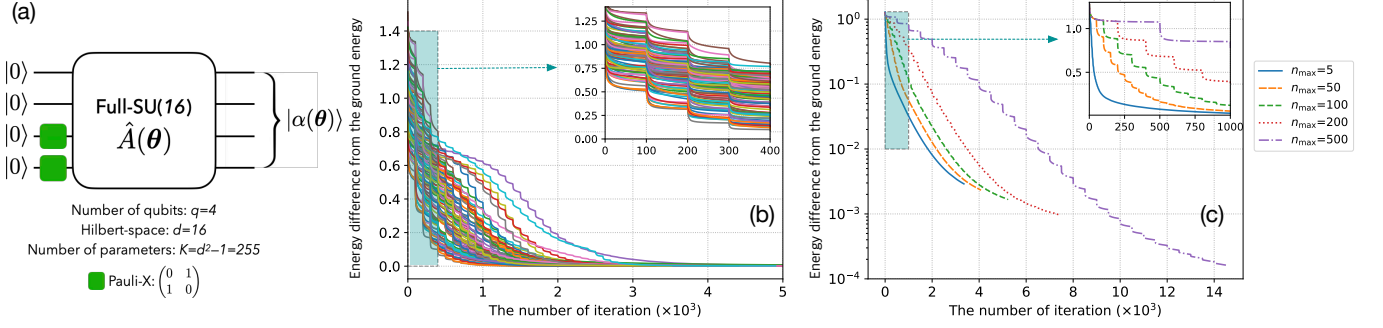


FIG. 6. QAAE for H_2 with a full $SU(16)$ ansatz. (a) The ansatz circuit $\hat{A}(\theta)$ is a full $SU(16)$ unitary, enabling exploration of the entire 16-dimensional Hilbert space ($K = 16^2 - 1 = 255$ parameters). (b) QAAE over 100 random initializations (applied to the 4-qubit Hartree-Fock reference $|0011\rangle$) exhibits robust, monotone improvement consistent with the analysis in Sec. III. (c) Effect of limiting state-learning effort per round to $n_{\max} \in \{500, 200, 100, 50, 5\}$: smaller n_{\max} accelerates early-stage progress but requires more rounds to reach high-precision estimates.

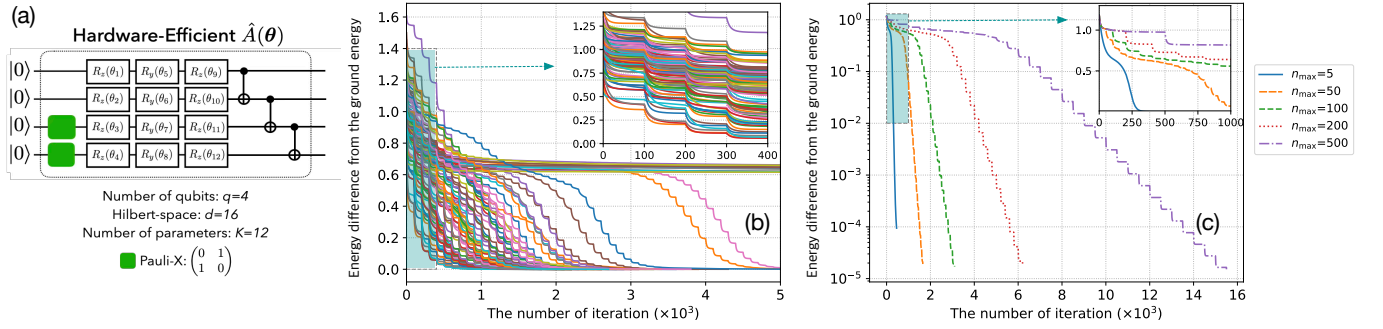


FIG. 7. QAAE for H_2 with a hardware-efficient ansatz. (a) Two-layer hardware-efficient circuit $\hat{A}(\theta)$ (single-qubit rotations + CNOT entanglers); $K = 24$ parameters. (b) Over 100 random seeds with $n_{\max} = 100$, about 90% reach the ground state; the remaining 10% stall due to limited expressivity and state-learning. (c) Varying $n_{\max} \in \{500, 200, 100, 50, 5\}$ shows fast early-round gains for small n_{\max} , with the final accuracy less sensitive to n_{\max} than in the $SU(16)$ case.

B. Hydrogen molecule

As a first molecular application, we target the ground state of H_2 . Here, we employ a four-qubit Hamiltonian \hat{H}_{H_2} obtained from second-quantized electronic structure in STO-3G followed by a Jordan-Wigner mapping [53]; the internuclear separation is fixed to 0.7\AA . Within QAAE, (A.1) implements the amplitude-amplification round using $\hat{A}(\theta)$, \hat{U} , \hat{R}_0 , and $\hat{T}(\theta)$; (A.2) performs the state-learning to re-encode the amplified target state.

Learning objective and halting.—For (A.2), we adopt stochastic gradient descent on the distance-based objective $\mathcal{F}(D)$, given in Eq. (19). Here, $D = \frac{1}{2} \|\hat{\rho}_{\text{out},k} - \hat{\rho}_{\theta'}\|_1$, which is the trace distance between the amplified target $\hat{\rho}_{\text{out},k} = |\varphi_{\text{out},k}\rangle\langle\varphi_{\text{out},k}|$ and the next-round trial $\hat{\rho}_{\theta'} = |\alpha(\theta')\rangle\langle\alpha(\theta')|$. The barrier term in Eq. (19) regularizes large-distance regions while keeping a well-conditioned minimum at the target [41]. The procedure halts at round r when

$$\Delta_{r-1,r} = |E_r - E_{r-1}| \leq \epsilon_H, \quad (30)$$

where $E_r = \langle\alpha(\theta_r)|\hat{H}_{H_2}|\alpha(\theta_r)\rangle$. Here, $\epsilon_H = 10^{-6}$. Note that the energy E_r here is used only as a stopping certificate; it is not the objective optimized within the loop.

Full $SU(d)$ ansatz (expressivity upper bound).—We adopt the ansatz operation $\hat{A}(\theta) \in SU(d)$ with $d = 16$. Although such circuits are impractical for large-scale chemistry, they provide a clean lens on (A.1)–(A.2) dynamics without expressivity bottlenecks. Initializing from the Hartree-Fock determinant, numerical runs across 100 random seeds show that the ground-state weight in $|\alpha(\theta)\rangle$ increases round-by-round, in line with **Proposition 1** and the logistic-type bound derived in Sec. III; see Fig. 6(b). We then cap the learning budget per round at n_{\max} gradient steps. As shown in Fig. 6(c), small n_{\max} yields a greedy regime—rapid initial energy drop due to repeated re-encoding of partially learned states—followed by a plateau that dissolves once additional learning steps are allowed. This quantifies a practical speed-vs-accuracy trade-off: early rounds can prioritize speed (small n_{\max}), while later rounds allocate more learning to sharpen the estimate.

Hardware-efficient ansatz (NISQ-oriented).—We next adopt a two-layer hardware-efficient circuit (single-qubit

rotations and CNOT entanglers; control parameters $K = 24$), which is natural for NISQ devices but cannot span the full Hilbert space. In this setting, (A.1) still supplies a state-independent overlap gain, while (A.2) may fail to perfectly re-encode the amplified target when the target leaves the ansatz manifold. Numerically, with $n_{\max} = 100$, approximately 90% of 100 random seeds converge to the ground state; the remaining 10% display stagnation attributable to expressivity-limited learning (see Fig. 7(b)). As in the SU(16) study, reducing n_{\max} accelerates early improvements (Fig. 7(c)), but here the terminal accuracy is comparatively less sensitive to n_{\max} , reflecting that the dominant limitation is expressivity rather than learning budget.

Across both ansatz families, QAAE maintains its non-variational identity: the loop does not minimize $\langle \Psi | \hat{H} | \Psi \rangle$ nor its gradients; it learns a fixed pure state produced by the coherent amplification. This avoids explicit exploration of rugged energy landscapes, while preserving hardware compatibility through short-time simulation in \hat{U} and modular control of \mathcal{D}_A . In practice, one can schedule n_{\max} to emphasize fast progress early and high precision late, and select ansatz families (chemistry-inspired vs. hardware-efficient) according to the target system and device constraints.

C. LiH molecule

As a second molecular test, we compute the potential energy curve (PEC) of lithium hydride (LiH) [8] and assess QAAE across bond lengths. Here, we use a 12-qubit second-quantized Hamiltonian \hat{H}_{LiH} obtained in the STO-3G basis with a Jordan–Wigner mapping (normalized as $\frac{1}{16}\hat{H}_{\text{LiH}}$) [53]. As in the previous H_2 example, (A.1) performs amplitude amplification and (A.2) state-learning re-encodes the amplified target in a chosen ansatz—here, unitary coupled-cluster singles and doubles (UCCSD). The learning uses stochastic gradient descent on $\mathcal{F}(D)$ in Eq. (19); to emulate tight hardware budgets we cap the learning effort per round at $n_{\max} = 5$.

Setup and protocol.—For each bond length $R \in [1.0, 3.3]\text{\AA}$, we initialize the UCCSD circuit $\hat{A}(\theta)$ on the Hartree-Fock reference. Each QAAE round executes one amplify step to generate $|\varphi_{\text{out},k}\rangle$, measures the observables needed for $\mathcal{F}(D)$, and performs at most $n_{\max} = 5$ learning steps to re-encode the amplified target as $|\alpha(\theta')\rangle$. The energy $E(R) = \langle \alpha(\theta) | \hat{H}_{\text{LiH}} | \alpha(\theta) \rangle$ is recorded for monitoring and halting, yet not the optimization objective within the loop.

Results and accuracy.—Figure 8 shows that the PEC (blue) converges monotonically toward the exact curve (red dashed) across the scan. The equilibrium bond length is recovered at $R = 1.5\text{\AA}$. With a total of 3,500 predicted trial states across the scan, the energy error at equilibrium is 1.8×10^{-5} Ha, while at $R = 3.2\text{\AA}$ (near dissociation) it is 1.6×10^{-3} Ha. The dissociation energy extracted from the QAAE PEC is 0.0958 Ha; for

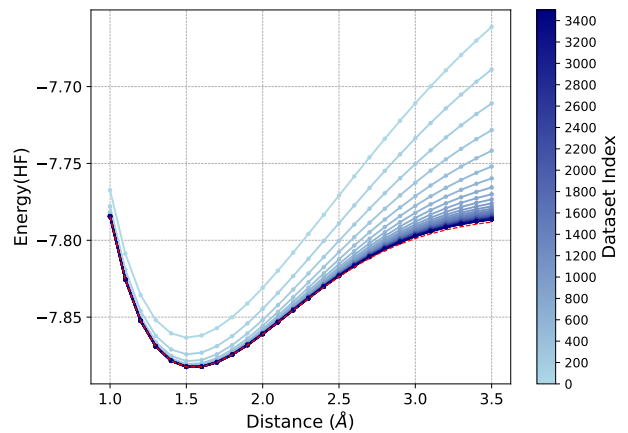


FIG. 8. LiH potential energy curve with UCCSD ansatz (12 qubits). Bond scan from 1.0\AA to 3.3\AA . Blue traces show per-round QAAE estimates (earliest rounds in lighter shades); the red dashed line is the exact ground-state energy for our 12-qubit model. QAAE drives the PEC toward the exact curve under a small learning budget $n_{\max} = 5$, illustrating landscape-free convergence with a chemistry-inspired ansatz.

our 12-qubit model the exact value is 0.0942 Ha, and the experimental reference is 0.0922 Ha. These data indicate that even under a very small learning budget per round, QAAE’s coherent amplification yields a quantitatively reliable PEC, approaching chemical-accuracy scales near the dissociation tail.

UCCSD supplies chemically structured expressivity, while QAAE’s amplify–learn loop provides directionality without energy-landscape exploration. The combination achieves robust, hardware-conscious convergence: short-time simulation in \hat{U} controls depth (Sec. III), and the limited learning budget trades a modest increase in rounds for stable, monotone PEC refinement.

D. Ising model in transverse and longitudinal fields

Finally, for a more practical application, we cast the 1D longitudinal–transverse-field Ising model (LTFIM),

$$\hat{H}_{\text{LTFIM}} = \sum_{j=1}^{N-1} \hat{\sigma}_z^{(j)} \hat{\sigma}_z^{(j+1)} + \sum_{j=1}^N (g \hat{\sigma}_x^{(j)} + h \hat{\sigma}_z^{(j)}), \quad (31)$$

where g and h are transverse and longitudinal fields, respectively. The model is integrable at $h = 0$ (via Jordan–Wigner) but becomes nonintegrable for $h \neq 0$ [54, 55]; its critical line connects $(g, h) = (1, 0)$ to $(0, 2)$ [56]. As such, LTFIM furnishes a stringent test bed that spans from exactly solvable to quantum-chaotic regimes.

Two-qubit hardware demonstration.—We first perform a IBMQ cloud experiment on *hardware* with $N = 2$ ($g = 1$ and $h = 0$) using a single ancilla qubit to implement the QAAE rounds. The controlled short-time evolution \hat{U} is compiled by sandwiching a Trotterized

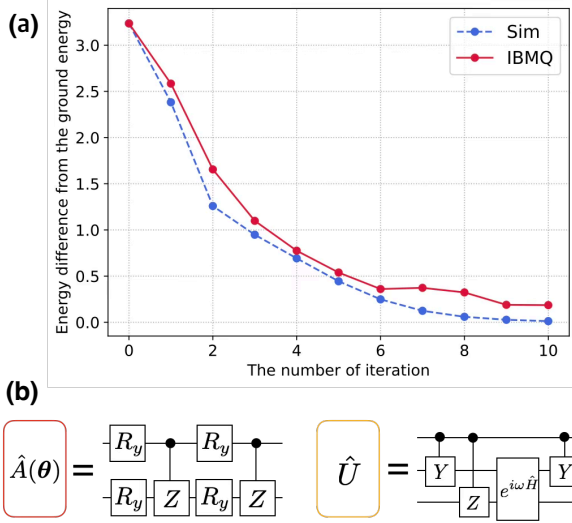


FIG. 9. Two-qubit model on IBMQ hardware ($N = 2$, and $(g, h) = (1, 0)$). (a) Energy error (relative to the exact ground energy) vs. QAAE rounds with $n_{\max} = 1$ learn-updates per round: experiment (“ibm_yonsei” IBMQ processor) vs. numerical emulation agree and decrease monotonically. (b) The hardware efficient ansatz $\hat{A}(\theta)$ and controlled evolution \hat{U} circuit used in the implementation.

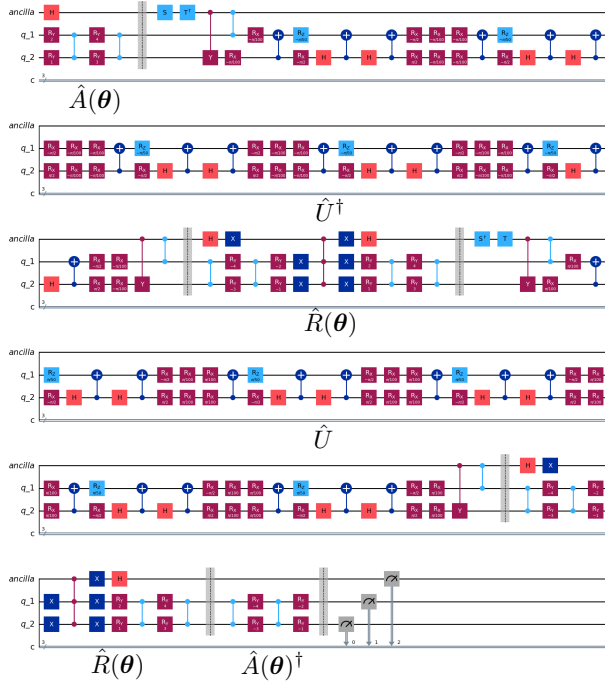


FIG. 10. The per-round QAAE circuit for IBMQ processor experiment: $N = 2$ and $(g, h) = (1, 0)$.

$e^{-i\omega\hat{H}}$ between controlled Pauli operations ($\hat{\sigma}_y^{(1)} \otimes \hat{\sigma}_z^{(2)}$), following the depth-reduction scheme of Ref. [44] (see the circuit in Fig. 9(b) and Fig. 10). Here, five second-order Trotter steps are used together with standard Qiskit optimization tool. Starting from a hardware-efficient ansatz

$\hat{A}(\theta)$ with an initial θ and a small initial ground-state overlap, the QAAE energy error decreases monotonically with the number of rounds, in close agreement with noiseless emulations (see Fig. 9(a)). This validates, *on real device* (“ibm_yonsei” IBMQ processor), that the amplify–learning loop provides the coherent improvement.

10-qubit regime and comparison to VQE.—We next probe a clearly nonintegrable LTFIM setting with $N = 10$ and $(g, h) = (1, 1)$. We emulate a normalized Hamiltonian $\frac{1}{2}(\frac{1}{20}\hat{H}_{\text{LTFIM}} + \hat{\mathbb{1}})$ and adopt a hardware-efficient ansatz built from layers of \hat{R}_y rotations and entangling CZ gates (2, 3, and 4 layers). For each setting, we average 100 random initializations. The state-learning per round is budget-limited to $n_{\max} \in \{100, 50, 10, 5, 1\}$ learning steps on the distance-based objective $\mathcal{F}(D)$ [Eq. (19)]. Figure 11 plots the mean energy error vs. QAAE round and, for a fair baseline, a conventional VQE that uses the same ansatz, optimizer, and stopping rule.

The results are as follows (see Fig. 11): (i) Early-stage speed: Smaller n_{\max} yields faster initial error reduction because repeated amplify–learn cycles leverage the coherent overlap gains even with partially learned parameters. (ii) Final accuracy and robustness: With sufficient learning budget, QAAE attains consistently lower final errors than VQE and with smaller dispersion across random seeds, whereas VQE often stalls at a higher error floor even after $\sim 10^4$ trial states. (iii) Resource fairness: Since both methods share the same ansatz and optimizer, the gap reflects algorithmic differences. That is, QAAE learns a fixed pure target each round and does not optimizes $\langle \Psi | \hat{H} | \Psi \rangle$; VQE, in contrast, navigates a rugged energy landscape with gradient estimates that can be fragile in depth and noise. Collectively, these results show that QAAE can surpass the gradient-gradient-based VQE in accuracy and reliability for a nonintegrable spin model while remaining the hardware-conscious.

V. DISCUSSION

In this work, we have developed and introduced the quantum amplitude-amplification eigensolver (QAAE), a ground-state (or energy) extraction framework that advances a trial state by coherently amplifying its ground-state component and then learning the resulting pure target at each round. Note that this is not an energy-landscape search but an amplify–learn pipeline: a state-independent overlap gain supplied by coherent amplitude amplification, followed by a state-learning step that re-encodes the amplified target into the chosen ansatz. Our analysis established a monotone improvement of ground-state overlap under standard assumptions (normalized Hamiltonian, nondegenerate ground-state, a faithful learning) and provided per-round depth bounds that scale with the ansatz and short-time simulation cost, ensuring hardware compatibility. We validated the mechanism on IBMQ hardware (two-level system and a two-qubit Ising model with an ancilla), and we

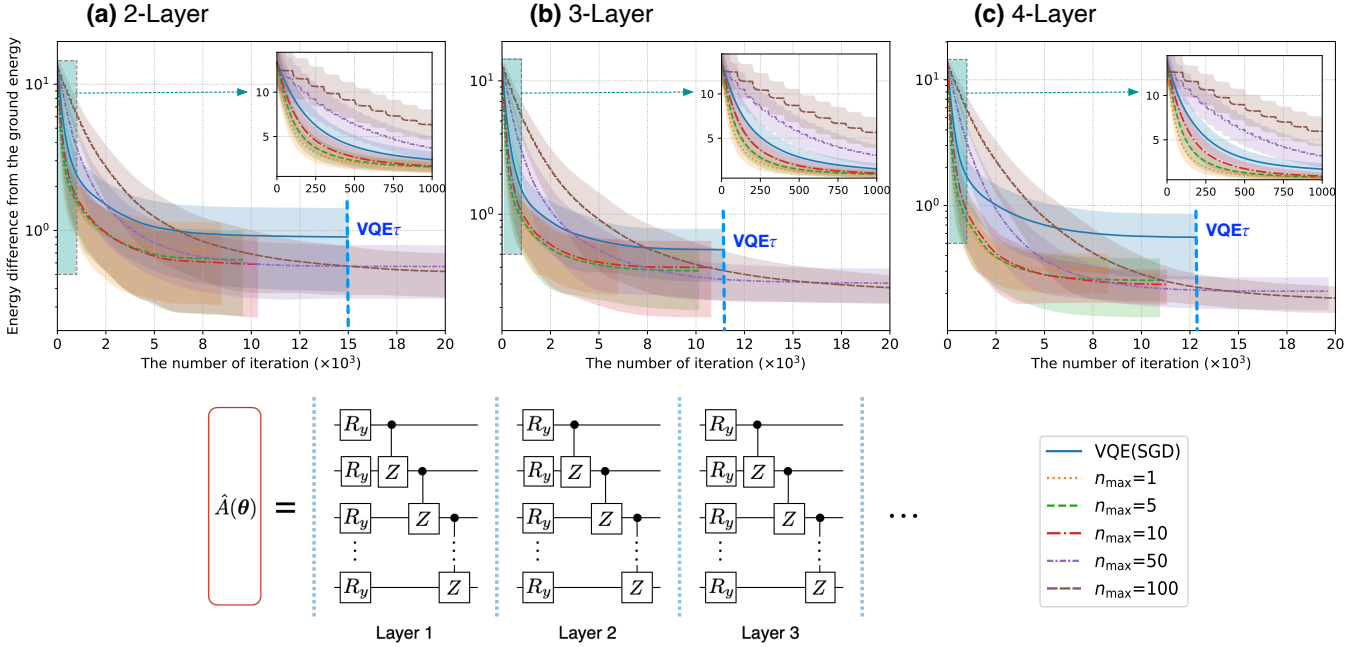


FIG. 11. LTFIM ($N = 10$ and $(g, h) = (1, 1)$) with the hardware-efficient ansatz: (a) 2, (b) 3 and (c) 4 layers. Mean energy error (solid line) \pm s.d. (shaded) over 100 random seeds. The colors denote $n_{\max} \in \{100, 50, 10, 5, 1\}$. For reference, VQE (same ansatz, optimizer, and halting rule) is overlaid. Across the depths, QAAE reaches lower errors and exhibits less variance than VQE; small n_{\max} accelerates early progress but can plateau earlier, quantifying a practical speed-accuracy trade-off.

benchmarked QAAE on H_2 , LiH, and a 10-qubit LTFIM, where it surpassed gradient-descent VQE in accuracy and reliability while remaining depth-conscious. These results position QAAE as a principled, non-variational, and landscape-free route to the ground-state estimation for near-term quantum simulation.

Understanding of QAAE’s convergence behavior clarifies how its principle departs from the conventional variational approaches. The variational eigensolvers minimize $\langle \Psi | \hat{H} | \Psi \rangle$ over a parameterized search space; progress is governed by the Hamiltonian’s energy landscape and the ansatz trainability of the ansatz. QAAE proceeds differently: the target is a fixed pure state produced by amplitude amplification, and learning amounts to a unitary re-encoding of that target within the ansatz family. Because the learning step targets a pure state, one may adopt distance-based objectives augmented with barrier regularization, avoiding pathological regions while keeping the target a well-conditioned minimizer. Thus, QAAE dispenses with energy or gradient estimators and does not traverse rugged energy landscapes, thereby reducing exposure to local minima that arise in energy-driven searches. The induced dynamics—monotone growth of ground-state overlap interleaved with the learning and controlled re-encoding—are qualitatively distinct (cf. Fig. 2), and are formalized by our ground-overlap gain proposition together with the stability bounds for the learning step.

Per-round circuit depth decomposes into preparation of the trial state (\mathcal{D}_A), a reflection about that state (\mathcal{D}_R),

and a controlled short-time evolution under \hat{H} (\mathcal{D}_U). The corresponding bound scales as $5\mathcal{D}_A + 2(\mathcal{D}_R + \mathcal{D}_U)$ with $\mathcal{D}_R \leq 2\mathcal{D}_A + \mathcal{O}(q)$ and $\mathcal{D}_U = \mathcal{O}(\text{poly}(q)\epsilon_H^{-1/2\kappa})$, so the implementability is dictated chiefly by the ansatz architecture and the simulation primitive for $e^{-i\omega\hat{H}}$ (Trotter/QSP/LCU). In practice, the chemistry-inspired (e.g., UCCSD) and hardware-efficient ansatz can both be embedded in QAAE; the former provides chemically structured expressivity, while the latter offers shallow and device-tailored circuits for NISQ experiments. This flexibility underpins our polynomial-depth implementations across the studied systems.

The QAAE’s guarantees rest on (i) normalized \hat{H} with a nondegenerate ground level, (ii) accurate short-time simulation $e^{-i\omega\hat{H}}$, and (iii) faithful learning/re-encoding in the chosen ansatz. The expressivity limits can slow or stall the learning if the amplified target exits the ansatz manifold; our experiments quantify this trade-off and show that scheduling the per-round learning budget n_{\max} (greedy in early rounds, precise in later rounds) provides practical control. As devices improve, error-mitigation and/or noise-aware objective shaping (e.g., normalization of the measured Pauli vectors) can further bolster robustness, as already observed in our hardware runs.

Looking ahead, QAAE invites several focused extensions. First, the learning step for pure-state targets can be refined via geometry-aware, distance-based objectives with barrier terms, adaptive per-round learning budgets, and noise-aware normalization of the measured observ-

ables. Second, we can exploit a partial structure of \hat{H} —symmetries, locality, or approximate spectra—to restrict the re-encoding manifold and accelerate the convergence. Lastly, it would be possible to curb the per-round depth by improving short-time simulation (e.g., higher-order Trotter, QSP/LCU with lightweight block encodings). We expect these directions to broaden QAAE’s reach across chemistry, materials, and many-body physics on increasingly capable devices.

ACKNOWLEDGEMENT

JB thanks Dr. Antonio Mandarino. JB and MSK thanks Jinzhao Sun for discussions. This work was supported by the Ministry of Science, ICT and Future Planning (MSIP) by the National Research Foundation of Korea (RS-2024-00432214, RS-2025-03532992, and RS-2023-NR119931), the Institute of Information and Communications Technology Planning and Evalu-

ation grant funded by the Korean government (RS-2019-II190003, “Research and Development of Core Technologies for Programming, Running, Implementing and Validating of Fault-Tolerant Quantum Computing System”), the Korean ARPA-H Project through the Korea Health Industry Development Institute (KHIDI), funded by the Ministry of Health & Welfare, Republic of Korea (RS-2025-25456722), and the Ministry of Trade, Industry, and Energy (MOTIE), Korea, under the project “Industrial Technology Infrastructure Program” (RS-2024-00466693). MSK acknowledges the UK EPSRC EP/W032643/1 and EP/Z53318X/1, the KIST through Open Innovation fund and the National Research Foundation of Korea (NRF) grant funded by the Korean Government (MSIT) (RS-2024-00413957). The entirety of SL’s contribution to the present work was completed while affiliated with his former institution, Electronics and Telecommunications Research Institute (ETRI). We acknowledge the Yonsei University Quantum Computing Project Group for providing support and access to the Quantum System One (Eagle Processor), which is operated at Yonsei University.

-
- [1] I. M. Georgescu, S. Ashhab, and F. Nori, Quantum simulation, *Reviews of Modern Physics* **86**, 153 (2014).
 - [2] J. Kempe, A. Kitaev, and O. Regev, The complexity of the local hamiltonian problem, *Siam journal on computing* **35**, 1070 (2006).
 - [3] U. Schollwöck, The density-matrix renormalization group, *Reviews of modern physics* **77**, 259 (2005).
 - [4] R. Orús, A practical introduction to tensor networks: Matrix product states and projected entangled pair states, *Annals of physics* **349**, 117 (2014).
 - [5] G. Vidal, Efficient simulation of one-dimensional quantum many-body systems, *Physical review letters* **93**, 040502 (2004).
 - [6] Otherwise the average sign decays—often exponentially in system size or inverse temperature—sending variances skyrocketing [57].
 - [7] D. S. Abrams and S. Lloyd, Quantum algorithm providing exponential speed increase for finding eigenvalues and eigenvectors, *Physical Review Letters* **83**, 5162 (1999).
 - [8] A. Aspuru-Guzik, A. D. Dutoi, P. J. Love, and M. Head-Gordon, Simulated quantum computation of molecular energies, *Science* **309**, 1704 (2005).
 - [9] B. L. Higgins, D. W. Berry, S. D. Bartlett, H. M. Wiseman, and G. J. Pryde, Entanglement-free heisenberg-limited phase estimation, *Nature* **450**, 393 (2007).
 - [10] L. Lin and Y. Tong, Heisenberg-limited ground-state energy estimation for early fault-tolerant quantum computers, *PRX quantum* **3**, 010318 (2022).
 - [11] G. H. Low and I. L. Chuang, Optimal hamiltonian simulation by quantum signal processing, *Physical review letters* **118**, 010501 (2017).
 - [12] A. M. Childs, Y. Su, M. C. Tran, N. Wiebe, and S. Zhu, Theory of trotter error with commutator scaling, *Physical Review X* **11**, 011020 (2021).
 - [13] R. B. Griffiths and C.-S. Niu, Semiclassical fourier transform for quantum computation, *Physical Review Letters* **76**, 3228 (1996).
 - [14] S. Fomichev, K. Hejazi, M. S. Zini, M. Kiser, J. Fraxanet, P. A. M. Casares, A. Delgado, J. Huh, A.-C. Voigt, J. E. Mueller, *et al.*, Initial state preparation for quantum chemistry on quantum computers, *PRX Quantum* **5**, 040339 (2024).
 - [15] G. Lee, M. Kang, J. Hong, S. Fomichev, and J. Huh, Filtered quantum phase estimation, *arXiv preprint arXiv:2510.04294* (2025).
 - [16] M. Cerezo, A. Arrasmith, R. Babbush, S. C. Benjamin, S. Endo, K. Fujii, J. R. McClean, K. Mitarai, X. Yuan, L. Cincio, *et al.*, Variational quantum algorithms, *Nature Reviews Physics* **3**, 625 (2021).
 - [17] K. Bharti, A. Cervera-Lierta, T. H. Kyaw, T. Haug, S. Alperin-Lea, A. Anand, M. Degroote, H. Heimonen, J. S. Kottmann, T. Menke, *et al.*, Noisy intermediate-scale quantum algorithms, *Reviews of Modern Physics* **94**, 015004 (2022).
 - [18] A. Peruzzo, J. McClean, P. Shadbolt, M.-H. Yung, X.-Q. Zhou, P. J. Love, A. Aspuru-Guzik, and J. L. O’Brien, A variational eigenvalue solver on a photonic quantum processor, *Nature communications* **5**, 4213 (2014).
 - [19] A. Kandala, A. Mezzacapo, K. Temme, M. Takita, M. Brink, J. M. Chow, and J. M. Gambetta, Hardware-efficient variational quantum eigensolver for small molecules and quantum magnets, *nature* **549**, 242 (2017).
 - [20] J. Tilly, H. Chen, S. Cao, D. Picozzi, K. Setia, Y. Li, E. Grant, L. Wossnig, I. Rungger, G. H. Booth, *et al.*, The variational quantum eigensolver: a review of methods and best practices, *Physics Reports* **986**, 1 (2022).
 - [21] J. R. McClean, J. Romero, R. Babbush, and A. Aspuru-Guzik, The theory of variational hybrid quantum-classical algorithms, *New Journal of Physics* **18**, 023023

- (2016).
- [22] X. Yuan, S. Endo, Q. Zhao, Y. Li, and S. C. Benjamin, Theory of variational quantum simulation, *Quantum* **3**, 191 (2019).
- [23] In VQE, the quantum processor supplies (noisy) unbiased estimates of $E(\theta)$ and its gradients, while a classical routine (e.g., SPSA/Adam/COBYLA) updates θ ; see Ref. [58] for surveys of hybrid workflows.
- [24] K. M. Nakanishi, K. Fujii, and S. Todo, Sequential minimal optimization for quantum-classical hybrid algorithms, *Physical Review Research* **2**, 043158 (2020).
- [25] D. Wierichs, C. Gogolin, and M. Kastoryano, Avoiding local minima in variational quantum eigensolvers with the natural gradient optimizer, *Physical Review Research* **2**, 043246 (2020).
- [26] J. R. McClean, S. Boixo, V. N. Smelyanskiy, R. Babbush, and H. Neven, Barren plateaus in quantum neural network training landscapes, *Nature communications* **9**, 4812 (2018).
- [27] M. Cerezo, A. Sone, T. Volkoff, L. Cincio, and P. J. Coles, Cost function dependent barren plateaus in shallow parametrized quantum circuits, *Nature communications* **12**, 1791 (2021).
- [28] A. A. Mele, G. B. Mbeng, G. E. Santoro, M. Collura, and P. Torta, Avoiding barren plateaus via transferability of smooth solutions in a hamiltonian variational ansatz, *Physical Review A* **106**, L060401 (2022).
- [29] L. Bittel and M. Kliesch, Training variational quantum algorithms is np-hard, *Physical review letters* **127**, 120502 (2021).
- [30] S. Wang, E. Fontana, M. Cerezo, K. Sharma, A. Sone, L. Cincio, and P. J. Coles, Noise-induced barren plateaus in variational quantum algorithms, *Nature communications* **12**, 6961 (2021).
- [31] S. Sim, P. D. Johnson, and A. Aspuru-Guzik, Expressibility and entangling capability of parameterized quantum circuits for hybrid quantum-classical algorithms, *Advanced Quantum Technologies* **2**, 1900070 (2019).
- [32] Z. Holmes, K. Sharma, M. Cerezo, and P. J. Coles, Connecting ansatz expressibility to gradient magnitudes and barren plateaus, *PRX quantum* **3**, 010313 (2022).
- [33] D. Wecker, M. B. Hastings, and M. Troyer, Progress towards practical quantum variational algorithms, *Physical Review A* **92**, 042303 (2015).
- [34] O. Crawford, B. van Straaten, D. Wang, T. Parks, E. Campbell, and S. Brierley, Efficient quantum measurement of pauli operators in the presence of finite sampling error, *Quantum* **5**, 385 (2021).
- [35] J. Bang, S.-W. Lee, C.-W. Lee, and H. Jeong, A quantum algorithm for obtaining the lowest eigenstate of a hamiltonian assisted with an ancillary qubit system, *Quantum Information Processing* **14**, 103 (2015).
- [36] S. Lloyd, Universal quantum simulators, *Science* **273**, 1073 (1996).
- [37] G. Brassard, P. Hoyer, M. Mosca, and A. Tapp, Quantum amplitude amplification and estimation, *Contemporary Mathematics* **305**, 53 (2002).
- [38] A. Ambainis, Quantum search algorithms, *ACM SIGACT News* **35**, 22 (2004).
- [39] P. A. Ivanov, E. Kyoseva, and N. V. Vitanov, Engineering of arbitrary $u(n)$ transformations by quantum householder reflections, *Physical Review A* **74**, 022323 (2006).
- [40] H. Zhao, L. Lewis, I. Kannan, Y. Quek, H.-Y. Huang, and M. C. Caro, Learning quantum states and unitaries of bounded gate complexity, *PRX Quantum* **5**, 040306 (2024).
- [41] W. Forst and D. Hoffmann, *Optimization—theory and practice* (Springer Science & Business Media, 2010).
- [42] M. Saeedi and M. Pedram, Linear-depth quantum circuits for n-qubit toffoli gates with no ancilla, *Physical Review A—Atomic, Molecular, and Optical Physics* **87**, 062318 (2013).
- [43] D. W. Berry, G. Ahokas, R. Cleve, and B. C. Sanders, Efficient quantum algorithms for simulating sparse hamiltonians, *Communications in Mathematical Physics* **270**, 359 (2007).
- [44] Y. Dong, L. Lin, and Y. Tong, Ground-state preparation and energy estimation on early fault-tolerant quantum computers via quantum eigenvalue transformation of unitary matrices, *PRX quantum* **3**, 040305 (2022).
- [45] M. Ostaszewski, E. Grant, and M. Benedetti, Structure optimization for parameterized quantum circuits, *Quantum* **5**, 391 (2021).
- [46] R. Babbush, J. R. McClean, M. Newman, C. Gidney, S. Boixo, and H. Neven, Focus beyond quadratic speedups for error-corrected quantum advantage, *PRX quantum* **2**, 010103 (2021).
- [47] E. T. Campbell, Early fault-tolerant simulations of the hubbard model, *Quantum Science and Technology* **7**, 015007 (2021).
- [48] R. Zhang, G. Wang, and P. Johnson, Computing ground state properties with early fault-tolerant quantum computers, *Quantum* **6**, 761 (2022).
- [49] D. Layden, First-order trotter error from a second-order perspective, *Physical Review Letters* **128**, 210501 (2022).
- [50] J. Sun, P. Zeng, T. Gur, and M. Kim, High-precision and low-depth eigenstate property estimation: theory and resource estimation, *arXiv preprint arXiv:2406.04307* (2024).
- [51] I. Hamamura and T. Imamichi, Efficient evaluation of quantum observables using entangled measurements, *npj Quantum Information* **6**, 56 (2020).
- [52] H.-Y. Huang, R. Kueng, and J. Preskill, Predicting many properties of a quantum system from very few measurements, *Nature Physics* **16**, 1050 (2020).
- [53] S. McArdle, S. Endo, A. Aspuru-Guzik, S. C. Benjamin, and X. Yuan, Quantum computational chemistry, *Reviews of Modern Physics* **92**, 015003 (2020).
- [54] E. Lieb, T. Schultz, and D. Mattis, Two soluble models of an antiferromagnetic chain, *Annals of Physics* **16**, 407 (1961).
- [55] L. Šamaj and Z. Bajnok, *Introduction to the statistical physics of integrable many-body systems* (Cambridge University Press, 2013).
- [56] A. Ovchinnikov, D. Dmitriev, V. Y. Krivnov, and V. Cheranovskii, Antiferromagnetic ising chain in a mixed transverse and longitudinal magnetic field, *Physical review B* **68**, 214406 (2003).
- [57] M. Troyer and U.-J. Wiese, Computational complexity and fundamental limitations to fermionic quantum monte carlo simulations, *Physical review letters* **94**, 170201 (2005).
- [58] W. Lavrijsen, A. Tudor, J. Müller, C. Iancu, and W. De Jong, Classical optimizers for noisy intermediate-scale quantum devices, in *2020 IEEE international conference on quantum computing and engineering (QCE)* (IEEE, 2020) pp. 267–277.